In vivo cross-linking and transmembrane helix dynamics support a bidirectional non-piston model of signaling within *E. coli* EnvZ

Rahmi Yusuf[a,1], Tuyết Linh Nguyễn[a,1], Annika Heininger[b], Robert J. Lawrence[a], Benjamin A. Hall[c*] and Roger R. Draheim[a,d*]

[a]School of Pharmacy and Biomedical Sciences, University of Portsmouth, Portsmouth, PO1 2DT, England, UK; [b]Institute of Biochemistry, Biocenter, Goethe University Frankfurt, D-60438 Frankfurt, Germany; [c]MRC Cancer Unit, University of Cambridge, Cambridge, CB2 0XZ, England, UK; [d]Institute of Biological and Biomedical Science, University of Portsmouth, Portsmouth, PO1 2DT, England, UK

Running title: Non-piston transmembrane communication within *E. coli* EnvZ

[1]These authors contributed equally

*To whom correspondence should be addressed (B. A. H. or R. R. D.):

MRC Cancer Unit
University of Cambridge
Hutchison / MRC Research Centre
Box 197, Cambridge Medical Campus
Cambridge
CB2 0XZ
United Kingdom
tel: + 44 (0) 1223 763240
fax: + 44 (0) 1223 763241

University of Portsmouth
School of Pharmacy and Biomedical Sciences
St. Michael's Building
White Swan Road
Portsmouth
PO1 2DT
United Kingdom
tel: +44 (0)23 9284 2133
fax: +44 (0)23 9284 3565

word count (abstract): 250
word count (body): 4757

Abstract

In Gram-negative bacteria, porins span the outer membrane and control the influx of several prominent groups of antibiotics. Thus, it should not be surprising that expression of these porins is often altered in clinical isolates exhibiting multidrug resistance (MDR). The major regulator of porin expression in *Escherichia coli* is EnvZ, a canonical sensor histidine kinase (SHK). It allosterically processes periplasmic interactions with MzrA and cytoplasmic osmosensing into a single unified change in the ratio of its kinase and phosphatase activities. Unfortunately, the role of the EnvZ transmembrane domain (TMD) in bidirectional communication of these signals remains not well understood. Here, we employed *in vivo* sulfhydryl-reactivity to probe the dynamics of the TM2 helices and demonstrate that upon stimulus perception, only the region proximal to the periplasm undergoes conformational rearrangement. Furthermore, *in silico* coarse-grained molecular dynamics (CG-MD) simulations with aromatically tuned variants of EnvZ TM2 demonstrate the existence of both tilting and azimuthal rotational components to transmembrane communication while ruling out piston-type repositioning of TM2. Finally, in contrast to a similar analysis of TM1, we identified position-specific mutants possessing a “flipped” phenotype by dual-color fluorescent reporter analysis suggesting that both the periplasmic and cytoplasmic ends of TM2 are critical for maintenance of EnvZ signal output. Taken together, these data strongly support that EnvZ employs a non-piston-type mechanism during transmembrane communication. We conclude by discussing these results within the context of allosteric processing by EnvZ and propose that these results can be used to predict and classify transmembrane communication by various SHKs.

Importance

The EnvZ sensor histidine kinase serves as the major regulator of porin expression within *Escherichia coli*. A long-standing question is how stimulus perception by a bacterial receptor on one side of a biological membrane is transmitted to the opposite side of the membrane. To address this question, we monitored the dynamics of the transmembrane domain of EnvZ *in vivo* and coupled these results with *in silico* simulations of membrane-embedded EnvZ transmembrane domains. Taken together, these results demonstrate that detection of osmotic stress by the cytoplasmic domain of EnvZ results in non-piston communication across the inner membrane of *E. coli*. Thus, in addition to understanding how

92 EnvZ regulates porin balance and antibiotic influx, these results contribute to answering the long-
93 standing question of how transmembrane communication is performed by bacterial receptors. Our work
94 concludes with a framework that correlates receptor domain composition and signal transduction
95 mechanisms that could be employed by other research groups on their particular receptors of interest.
96

Keywords

porin balance / transmembrane communication / coarse-grained molecular dynamics / sulfhydryl-reactivity / transmembrane helix dynamics

Introduction

Most porins involved in antibiotic transport by Gram-negative bacteria belong to the classical OmpF and OmpC families (1). Transcription of these porins is governed by the intracellular concentration of phospho-OmpR (OmpR-P), which is controlled by EnvZ in response to changes in periplasmic interactions with MzrA and environmental osmolarity (2-7) (Fig. 1A). At low intracellular levels of OmpR-P, transcription of *ompF* is upregulated, whereas at higher levels of OmpR-P, transcription of *ompF* is repressed and transcription of *ompC* is activated. This results in a predominance of OmpF at low osmolarity and OmpC at higher osmolarities or in the presence of MzrA (8-10) (Fig. 1B). Dramatic modification of porin balance, which has been observed within clinical isolates from patients undergoing antibiotic treatment, strongly supports further characterization of the underlying mechanisms of porin regulation by EnvZ (11-17). In addition, it was recently shown that mutations in EnvZ within a porin-deficient (*ompC*$^-$ *ompF*$^-$) *E. coli* strain resulted in increased carbapenem resistance (18). Thus, in addition to maintenance of porin balance, EnvZ also plays another not well-understood role in mediating antibacterial resistance that warrants further elucidation.

A substantial body of evidence suggests that EnvZ participates in bidirectional allosteric processing. A cytoplasmic fragment of EnvZ ($EnvZ_c$), consisting of residues Arg-180 through Gly-450, has been shown to mediate physiologically appropriate responses to increasing NaCl and sucrose concentrations *in vitro* and to increasing sucrose *in vivo* (19). These results led the suggestion that the peripalsmic and transmembrane domains of EnvZ play a negligible role in osmosensing with the exception of anchoring EnvZ within the membrane and thereby reducing a three-dimensional search by OmpR to a two-dimensional search (19). In addition, it was initially suggested membrane anchoring might reduce the conformational dynamics of EnvZ to physiologically relevant levels, as $EnvZ_c$ was found to have greater specific activity than full-length membrane-bound EnvZ (19, 20). Further studies demonstrated that peripheral interactions between the cytoplasmic domains and the lipid membrane were essential in increasing the kinase activity of the cytoplasmic domain of EnvZ, including the observation of a roughly 25-fold in $EnvZ_c$ signal output while maintaining regulation, *i.e.* a 2-fold increase in autophosphorylation, in response to sucrose *in vitro* (21). In summary, these results confirm that molecular dynamics within the cytoplasmic domain of EnvZ govern response to osmolarity and that lipid-receptor interactions play a modulating the signal output of EnvZ.

Alternatively, MzrA, modulator of EnvZ and OmpR protein A, was identified as a suppressor of a Δ*bamB* Δ*degP* double mutation. Upon further analysis, it was shown that MzrA is an upstream regulator of EnvZ signal output that is independent of signal output modulation due to osmolarity, pH and procaine (6). MzrA was subsequently shown to localize to the inner membrane and interact with EnvZ within the peripalsmic space (7) to serve as a connector between the CpxA/CpxR and EnvZ/OmpR signaling circuits (6). It is also known as a connector of which only a few examples have been found (22-24).

When taken together, these results demonstrate that the TMD of EnvZ is responsible for allosterically coupling sensory input from the attached periplasmic and cytoplasmic domains. By extension, bidirectional communication through the TMD is required in order to properly modulate porin expression. Thus, we were interested in how cytoplasmic osmosensing could modulate the conformational dynamics of the TMD and subsequently that of the periplasmic domain. Understanding how EnvZ transduces signal across the biological membrane would be a significant step toward direct manipulation of porin balance in bacterial cells exhibiting MDR.

To address these lines of enquiry, we have created a single-Cys-containing library of EnvZ mutants across the second TM helix (TM2) that physically connects the periplasmic and the cytoplasmic domains of EnvZ. *In vivo* analysis of this library revealed three regions within the TM domain, of which the periplasmic region undergoes a non-piston-type conformational change. CG-MD simulations of the aromatically tuned and wild-type EnvZ TM2 variants supported these results. We conclude by discussing these results in the context of governance of porin balance and that mechanisms of transmembrane communication can be classified based on the periplasmic domains that the bacterial receptor possesses.

Results

Creating a single-Cys-containing library within TM2 of EnvZ

We previously created a Cys-less version of EnvZ from *E. coli* that had its sole Cys residue changed to an Ala residue (C277A). The Cys-less variant is expressed from pRD400, which results in the addition of a seven-residue linker (GGSSAAG) and a C-terminal V5 epitope (GKPIPNPLLGLDST). We previously found that the Cys-less version of EnvZ had similar steady-state signal output and response to environmental osmolarity as the wild-type version of EnvZ making it suitable for comparisons of *in vivo* sulfhydryl-reactivity and signal output analysis. We initially determined that no major rearrangements occur along the TM1-TM1' interface upon stimulus perception (25). As minimal change was observed along this helical interface in response to osmolarity, we continued by examining the TM2-TM2' interface. We began by determining which residues comprise TM2 by subjecting the full EnvZ sequence to DGpred (26) and TMHMM v2.0 (27), which suggested that Leu-160 to Ile-181 and Leu-160 to Ile-179 comprise TM2 respectively. Based on these analyses, we employed site-directed mutagenesis using the Cys-less variant as a template to create a library of single-Cys-containing EnvZ proteins that spanned from positions 156 to 184 (Fig. 2). We observed that nearly the entire library was expressed within EPB30/pRD400 cells grown under the low- or high-osmolarity regime. Variants possessing a Cys at position 156 showed low levels of expression when grown under the low-osmolarity (0% sucrose) regime. However, when grown under the high-osmolarity regime, no variants showed reduced expression level (Fig. S1). These results indicate that the library was suitable for further *in vivo* experimentation.

Mapping TM2 surfaces important for maintenance of EnvZ signal output

We began by expressing each of the single-Cys-containing variants in EPB30/pRD400 cells, which allowed us to measure CFP fluorescence, YFP fluorescence, and to calculate the CFP/YFP ratio that estimates steady-state EnvZ signal output (Fig. 1B). Cells expressing the Cys-less C277A were used as a baseline comparison (Fig. S2). When EPB30/pRD400 cells are grown under the low-osmolarity regime, a shift in signalling output toward the "on" or kinase-dominant state results in increased CFP fluorescence, reduced YFP fluorescence and an increase in the overall CFP/YFP ratio, while a shift toward the "off" or phosphatase-dominant state appears as decreased CFP, increased YFP and a decrease in CFP/YFP ratio (Fig. 3 and S3).

Several trends were observed during analysis of the library of Cys-containing EnvZ receptors. When

EPB30/pRD400 cells were grown under the low-osmolarity regime, EnvZ was less tolerant of Cys substitutions at the N- and C-terminal regions of the library. At the N-terminus, signal output from receptors containing a Cys at positions 156, 162 and 163 were very elevated, exhibiting greater than a 5-fold increase in CFP/YFP, while receptors possessing a Cys in the C-terminus at positions 179, 181, 182 and 184 were elevated, possessing over a 2-fold increase in CFP/YFP. These boundary regions appear to flank a core of alternating increases and decreases in EnvZ signal output, as observed between residue positions 165 and 180, suggesting that multiple tightly packed EnvZ helices exist within the hydrophobic core of the inner membrane (Fig. 3A and 3B). When grown under the high-osmolarity regime, a pattern appeared where Cys substitutions resulted in significant decreases in signal output (Fig. 3C). Of the 29 mutants analysed, 13 supported less than 75% of the normal wild-type signal output.

Most striking is the inverse effect on EnvZ signal output of the Cys substitutions that flank the hydrophobic core of TM2. For these residues, when grown under the low-osmolarity regime, the presence of a Cys resulted in an increase in signal output of more than 25%, i.e. shifted toward the on or kinase-dominant state (red dots in Fig. 3A) and a reduction in signal output of more than 25%, i.e. shifted toward the off or phosphate-dominant state, when grown under the high-osmolarity regime (blue dots in Fig. 3C). These flipped positions reside at the N- and C-terminal ends of the region we examined and outside of the proposed hydrophobic TMD core (Fig. 3). Within the hydrophobic core, Cys substitutions show similar changes when cells are grown under the low- and high-osmolality regimes. These results suggest that the flanking regions are not simply rigid structural conduits for signal transduction but may have higher-order roles in signal transduction, such as MzrA interaction or functioning as a control cable at the N- and C-terminal regions respectively (6, 7, 28-31).

Identifying surfaces involved in TM2-TM2' interactions

Sulfhydryl-reactivity experimentation is well-characterised and has been employed on many soluble and membrane-spanning proteins and higher-order complexes (32). The *in vivo* nature of this assay facilitated mapping of the TM2-TM2' interface under different osmotic conditions, which is an important first step toward understanding how EnvZ processes allosteric inputs from periplasmic MzrA binding and cytoplasmic osmosensing into a single uniform modulation of bacterial porin balance (Fig.

1). In a similar manner to mapping TM1-TM1' interactions (25), Cys-containing EnvZ variants were expressed in EPB30/pRD400 cells and upon entering the early exponential phase ($OD_{600nm} \approx 0.25$) they were subjected to 250 μM molecular iodine for 10 minutes analysed by non-reducing SDS-PAGE and immunoblotting (Fig. S4).

We observed three distinct regions within TM2. The N-terminal region (region I in Figure 3), comprised of residues 156 to 163, exhibited significant cross-linking under the low-osmolarity regime (0% sucrose) and almost no crosslinking under the high-osmolarity (15% sucrose) regime. The second region (II) consisting of positions 164 to 179, demonstrated altering low and high levels of disulphide-formation consistent the crossing of TM2 and TM2' within the hydrophobic core of the TMD. The final region (III), from residues 180 to 184, shows no crosslinking (Fig. 4). It should be noted that this significant difference at the periplasmic end of the TMD between cells grown under the low- and high-osmolarity regime was not observed during similar analyses of TM1 (25).

Molecular simulations of the wild-type and aromatically tuned variants of EnvZ TM2

The piston-type model of transmembrane communication is founded upon the central tenant that the vertical position of TM2 relative to the lipid bilayer changes upon stimulus perception. Previous work with TM2 of Tar demonstrates that repositioning the aromatic residues at the cytoplasmic end of TM2, known as aromatic tuning (33), repositions the helix within a biological membrane (34) and that this repositioning causes an incremental change in signal output (33). These results served as an experimental framework to optimise SIDEKICK software capable of high-throughput parallelised coarse-grained molecular dynamics (CG-MD) simulations, which demonstrated that aromatic tuning repositioned the TM2 helix *in silico* in a manner consistent with both the *in vivo* results and a piston-type mechanism of transmembrane communication (35).

Based on these extensive results and the recent suggestion that mechanisms employed by SHKs during TM communication correlate with the presence of a membrane-adjacent HAMP domain (36), we performed analogous *in silico* experimentation with EnvZ, which possesses a membrane-adjacent HAMP domain but substitutes a periplasmic PDC/CACHE domain for the four-helix bundle present in Tar and NarQ (36-39). We previously performed aromatic tuning with TM2 of EnvZ and found that

signal output was not correlated with the absolute vertical position of the aromatic residues as was shown with Tar TM2, which suggested that EnvZ does not transduce signal output across the membrane by a piston-type displacement (40).

Interpretation and assessment of the CG-MD results

To interpret the results of our GC-MD analysis, we categorised the signal output of these aromatically tuned EnvZ variants (40). For several two-component signalling circuits, including the EnvZ/OmpR, PhoQ/PhoP and CpxA/CpxR circuits, the steady-state output of the signalling circuits has been shown to be independent of the level of SHK present (40-43). However, in circuits containing the tuned variants of EnvZ, a different relationship between steady-state signal output and receptor level was observed, suggesting that the ratio of kinase to phosphatase activities was different within each receptor and always different than wild-type EnvZ (40). Based on this analysis, we found that the WLF-1 variant possessed the highest signal output while the WLF-5, WLF-4 and WLF-3 variants possessed slightly higher activity than wild-type EnvZ, which maintained receptor-concentration dependent robustness unlike the tuned variants. WLF-2 and WLF+1 were found to possess reduced signal output, while WLF+2 possessed the lowest overall signal output. These differences were previously quantified by analysing the slope of the change in CFP/YFP against the amount of receptor present and are visually represented in Figure S5 (40). These classifications are employed during interpretation of the CG-MD results in Figure 5.

Based on these previous results and the absence of asymmetric TM2 displacement observed within the *in vivo* sulfhydryl-reactivity assay (Fig. 4), we assessed whether molecular simulations would lend credibility to a non-piston type of transmembrane communication employed by EnvZ. We began by designing tuned TM2 sequences to subject to GC-MD simulations that matched those previously used during the aromatic tuning experimentation (Fig. 5A). Snapshots of individual frames and a movie from the CG-MD analysis with the wild-type EnvZ TM2 segment can be found in the Supporting Information (Fig. S6 and Movie S1). Unlike analogous experimentation with TM2 of Tar, no trend in helix displacement was observed (Fig. 5B, Table S1). This indicates that the mutations do not in isolation move the helix up and down in the membrane and would appear to rule out a pure piston motion as previously observed in Tar (35).

An alternative mechanism for transmembrane communication is to induce a tilt in the helix relative to the bilayer normal. This was originally proposed in Tar on the basis of crystallographic analysis of the receptor domain (44), and led to the proposal of a "swinging piston" where both displacement and tilt contributed to signal transduction. In addition, this would be consistent with a scissor-type model of TM communication proposed to be utilised by PhoQ (45, 46), which possesses a periplasmic PDC/CACHE domain (47). In testing the tuned EnvZ TM2 helices, a change in the extent of tilting was observed during the CG-MD simulations (Fig.5C, Table S2). It was found that a reduction in tilt, to a mean tilt of between 22 and 24 degrees, compared to the wild-type TM2 sequence with a tilt of approximately 26 degrees correlated with a decreased signal output (phosphatase-biased, dark blue). Interestingly, an increase in tilt to more than 29 degrees correlated with extremely biased signal output, *i.e.* kinase-dominant (WLF-1, bright red) and phosphatase-dominant (WLF+2, bright blue). Taken together, these results demonstrate that tilt, rather than vertical displacement, does correlate with modulated signal output from EnvZ.

Finally, a rotational/gearbox model of TMD-HAMP communication has also been proposed for EnvZ (48, 49). Central to this model is that interconversion between the kinase-dominant and phosphatase-dominant signalling states can be accomplished by rotation of individual HAMP helices by 26 degrees. With our simulations, we observed some consistency with this gearbox model of HAMP signalling, especially when the WLF-1 helix possessed a mean azimuthal rotation that is 25 degrees different than wild-type EnvZ (bright red in Figure 5D). In the full-length EnvZ WLF-1 receptor, this variant possessed the highest signal output. Further rotation of an additional 15 degrees for a total of 40 degrees from wild-type correlated with the most phosphatase-dominant receptor, WLF+2. For the other simulated helices, it was not possible to differentiate them into separate classes.

Discussion

Non-piston transmembrane communication by EnvZ

EnvZ has been shown to allosterically process cytoplasmic changes in osmolarity and upon interaction with MzrA within the periplasmic. Here, our *in vivo* analysis demonstrated that only the periplasmic

end of EnvZ TM2 undergoes a conformational transition upon cytoplasmic stimulus perception and suggests that the asymmetric piston-type displacement employed by Tar is not used by EnvZ. To our knowledge, this is the first example of a periplasmic end of TM2 being affected by a cytoplasmic stimulus observed within EnvZ. Various experimentation has also been performed with the aromatically tuned variants of TM2 from both Tar and EnvZ. Previously, a linear correlation was observed between the position of the aromatic residue in Tar TM2, the position of the helices *in vitro* and *in silico* and the signal output from each Tar receptor (33, 34, 40, 50). Here, *in silico* analysis of EnvZ TM2 demonstrates that such a linear correlation is absent and that EnvZ functions by a non-piston mechanism in which both tilting and azimuthal rotation play a substantial role in modulation of signal output (Figure 5).

Correlations between domain composition and transmembrane communication

Comparisons of recently published *apo* and *holo* high-resolution (~1.9 Å) crystal structures of the *E. coli* nitrate sensor NarQ that contain the periplasmic, TM and HAMP domains reveal extensive structural rearrangements involving a piston-like motion of TM1 relative to TM2 of approximately 2.5 Å. These displacements result in a lever-like rotation of individual HAMP domains upon binding of cognate ligand (36). Based on these results, the authors posit that receptors containing a membrane-adjacent HAMP domain function by a piston-type displacement of TM helices while those that lack such domains transduce signal by rotation of TM helices. We previously postulated a related yet different categorization of signaling mechanisms also based on the domain structure of bacterial receptors (51). We proposed that receptors containing a periplasmic four-helix bundle transduce signal across the membrane by piston-type displacements and that the attached membrane-adjacent HAMP domains might possess one of a multitude of signaling mechanisms including a gearbox-type rotation (48), a dynamic bundle (28) or potentially other mechanisms (51). Differentiating between these classification systems will provide a theoretical framework for understanding domain-based intra-protein allosteric communication by bacterial receptors. A recent authoritative structural-based review of transmembrane communication by bacterial receptors addresses these different suggestions (52).

This results presented here also examines whether SHKs that possess membrane-adjacent HAMP domains function solely by piston-type displacements or whether other signaling mechanisms might be

350 employed. The results here with EnvZ should be compared with previous findings from the aspartate
351 chemoreceptor (Tar) and the recent NarQ structures (36, 53-55) as these three are ideal candidates for
352 comparison because they all possess a membrane-adjacent HAMP domain, however, while Tar and
353 NarQ possess a periplasmic four-helix bundle, EnvZ possesses a periplasmic PDC/CACHE domain
354 (37, 38). The authors of the recent NarQ structures posit that the presence or absence of the membrane-
355 adjacent HAMP domain may be the difference between receptors employing piston-type mechanisms
356 of transmembrane communication as compared to other mechanisms (36). However, differences
357 employed during transmembrane communication by the Tar and EnvZ TMDs observed here and
358 previously strongly suggest that Tar and EnvZ possess different mechanism of TM communication
359 even though both possess a membrane-adjacent HAMP domain. Our previous work analyzed AS1
360 helices from *E. coli* NarX, *E. coli* Tar, *E. coli* EnvZ and Af1503, the HAMP domain resulting in the
361 initial high-resolution structure (48), and found that the Tar and NarX AS1 helices possess similar
362 properties, which the AS1 helices from both EnvZ and Af1503 fail to possess. Recent comparisons of
363 the *apo* and ligand-bound structures of the combined periplasmic-TM-HAMP domain from *E. coli*
364 NarQ demonstrate that binding of ligand results in symmetrical displacements of TM1 relative to TM2
365 of approximately 2.5 Å (36). These results are similar to Tar, which functions by asymmetrical TM2
366 displacement also possesses a periplasmic four-helix-bundle (39, 53-55).
367
368 *Conclusion*
369
370 Based on these results, we conclude that *E. coli* EnvZ functions by a non-piston mechanism of
371 transmembrane communication that is different than Tar, NarX and NarQ, which communicate across
372 the membrane by piston-type displacements. Furthermore, we propose that TM signaling mechanisms
373 can be predicted and assigned based upon the domain(s) present in the periplasmic region of a bacterial
374 membrane-spanning receptor.
375
376 **Materials and Methods**
377
378 *Bacterial strains and plasmids*
379

E. coli strains DH10B (New England Biolabs) or MC1061 (56) were used for DNA manipulations, while strain K-12 MG1655 (57) served a non-fluorescent strain that was used to control for light scattering and cellular autofluorescence. *E. coli* strains MDG147 [MG1655 Φ(*ompF*$^{+}$-*yfp*$^{+}$) Φ(*ompC*$^{+}$-*cfp*$^{+}$)] (58) and EPB30 (MDG147 *envZ::kan*) (43) were employed for analysis of EnvZ signal output. As the C-terminus of bacterial receptors can be sensitive to the presence of an epitope tag, we previously ensured that the addition of a V5-epitope tag did not alter the signaling properties of EnvZ (40, 59). Plasmid pEB5 was employed as an empty control vector (41). Plasmid pRD400 (40) retains the IPTG-based induction of EnvZ from plasmid pEnvZ (60) while adding a seven-residue linker (GGSSAAG) (61) and a C-terminal V5 epitope tag (GKPIPNPLLGLDST) (62). Plasmid pEB5 was employed as an empty control vector.

Selection of residues comprising TM2 of EnvZ

The primary sequence of EnvZ from *E. coli* K-12 MG1655 was subjected to DGpred using a minimal window of 9 residues and a maximal window of 40 residues (26). Alternatively, a software package that identifies TM helices with a Markov model (TMHMM v2.0) (27) was also employed. These software packages suggested that Leu-160 to Ile-181 and Leu-160 to Ile-179 comprise TM2 respectively. Based on these results and to maximize the probability of including all residues within TM2, we targeted all residues between positions 156 to 184 for the creation of a library of single-Cys-containing EnvZ receptors.

Analysis of EnvZ signal output in vivo

Bacterial cultures were grown as described previously (40) with minor modification. MDG147 or EPB30 cells were transformed with pRD400 expressing one of the single-Cys-containing EnvZ receptors or pEB5 (empty). Fresh colonies were used to inoculate 2-ml overnight cultures of minimal medium A (63) supplemented with 0.2% glucose. Ampicillin, sucrose and IPTG were added as appropriate. Cells were grown overnight at 37 °C and diluted at least 1:1000 into 7 ml of fresh medium. Upon reaching an $OD_{600nm} \approx 0.3$, chloramphenicol was added to a final concentration of 170 μg/ml. Fluorescent analysis was immediately conducted with 2 ml of culture and a Varian Cary Eclipse (Palo Alto, CA). CFP fluorescence was measured using an excitation wavelength of 434 nm and an emission

411 wavelength of 477 nm, while YFP fluorescence was measured using an excitation wavelength of 505
412 nm and an emission wavelength of 527 nm. These values were corrected for cell density and for light
413 scattering/cellular autofluorescence by subtracting the CFP and YFP fluorescence intensities
414 determined for MG1655/pEB5 cells.
415
416 *Analysis of sulfhydryl-reactivity* in vivo
417
418 Cells were grown as described above with minor chnges. Upon reaching an OD_{600nm} ~ 0.3, cells were
419 subjected to between 250 μM molecular iodine for 10 min while incubating at 37 °C. The reaction was
420 terminated with 8 mM N-ethylmaleimide (NEM) and 10 mM EDTA. Cells were harvested by
421 centrifugation and resuspended in standard 6X non-reducing SDS-PAGE buffer supplemented with
422 12.5 mM NEM. Cell pellets were analysed on 10% SDS/acrylamide gels. Standard buffers and
423 conditions were used for electrophoresis, immunoblotting and detection with enhanced
424 chemiluminescence (64). Anti-V5 (Invitrogen) was the primary antibody and peroxidase-conjugated
425 anti-mouse IgG (Sigma) was the secondary antibody. Digitized images were acquired with a ChemiDoc
426 MP workstation (Bio-RAD), analysed with ImageJ v1.49 (65) and quantified with QtiPlot v0.9.8.10.
427
428 *CG-MD simulations with SIDEKICK*
429
430 As previously described (35), coarse-grained molecular dynamics (CG-MD) simulations were
431 performed using the MARTINI forcefield with an approximately 4:1 mapping of non-H atoms to CG
432 particles. Lennard-Jones interactions between 4 classes of particles: polar (P), charged (Q), mixed
433 polar/apolar (N) and hydrophobic apolar (C) were used to treat interparticle interactions. Within
434 MARTINI, P and C particle types were subdivided to reflect varying degrees of polarity. Short range
435 electrostatic interactions were treated Coulombically, shifted to zero between 0 and 12 Å. Lennard-
436 Jones interactions were shifted to zero between 9 and 12 Å. α-helix integrity was maintained via
437 dihedral restraints. Peptide termini were treated as uncharged. Simulations were performed using
438 Gromacs 3 (66). Temperature was coupled using a Berendsen thermostat at 323 K (τ_T = 1 ps), and
439 pressure was coupled semi-isotropically (across XY/Z) at 1 bar (compressibility = 3×10^{-5} bar^{-1},
440 τ_P = 10 ps). The initial simulation timestep was 20 fs. Initial models of the TM α-helices were
441 generated as ideal, atomistically detailed α-helices using standard backbone angles and side- chain

conformers. These were then converted to coarse-grained as described previously(35). Around 128 DPPC molecules were used in each simulation along with around 3000 CG water particles, giving a final system size of □65×65×13 Å.

Acknowledgments

R. Y. was generously supported by the Indonesia Endowment Fund for Education, Ministry of Finance (S-4833/LPDP.3/2015). T. L. N. was supported by a grant from the Erasmus+ programme. R. R. D. was supported with start-up funding from the Faculty of Science and from the Institute of Biological and Biomedical Science (IBBS) at the University of Portsmouth. B. A. H. was supported by The Royal Society (UF130039).

Figure legends

Figure 1. Monitoring modulation of EnvZ signal output upon stimulus perception. (A) EnvZ signal output controls porin expression. It is a bifucntional sensor histidine kinase with both kinase and phosphatase activities. The ratio of these activities is modulated by the presence of extracellular osmolarity and the absence/presence of MzrA (blue). (B) The intracellular level of phosphorylated OmpR (OmpR-P) is controlled by EnvZ signal output and OmpR-P levels govern transcription of *ompF* and *ompC*. Strains MDG147 and EPB30 (Δ*envZ*) contain transcriptional fusions of *yfp* to *ompF* (yellow) and *cfp* to *ompC* (cyan), which facilitates easy monitoring of intracellular OmpR-P levels by measuring the CFP/YFP ratio. The dashed line indicates an estimation of the baseline OmpR-P levels from EPB30/pRD400 cells grown under the low-osmolarity regime (0% sucrose).

Figure 2. EnvZ functions as a homodimer with a cytoplasmic N-terminus, the first transmembrane helix (TM1, white), a large periplasmic domain (sensor, white), the second transmembrane helix (TM2, red), a membrane-adjacent HAMP domain (grey) and the cytoplasmic domains responsible for dimerization and histidylphosphortransfer (DHp, black) and catalytic ATPase activity (CA, black). The position of the original Cys-277 residue that was mutated to Ala to produce the Cys-less EnvZ is provided. The residues subjected to Cys substitution and their position in the primary sequence is provided. Signal output from each single-Cys-containing variant is compared to the Cys-less (C277A) variant: less than

50% of Cys-less (light blue), between 50% and 75% of Cys-less (dark blue), between 75% and 125% of Cys-less (grey), between 125% and 200% (dark red) and greater than 200% (light red). Residue positions exhibited flipped signal output are indicated with a plus. The extent of sulphydryl-reactivity is also presented in five categories based on dimer-to-monomer ratio: no dimer present (white), less than 0.05 (light grey), between 0.05 and 0.2 (medium grey), between 0.2 and 0.5 (dark grey) and greater than 0.5 (red). Positions that exhibit a significant change in cross-linking between the low- and high-osmolarity regimes are indicated with a plus.

Figure 3. Signal output from the library of single-Cys EnvZ variants. (A) CFP/YFP from EPB30/pRD400 cells expressing one of single-Cys variants grown under the low-osmolarity (0% sucrose) regime. On the right axis, these CFP/YFP ratios are compared to the Cys-less (C277A) variant. (B) Magnified version of panel A in order to emphasise the region up to a 2-fold increase in CFP/YFP. (C) CFP/YFP from EPB30/pRD400 cells expressing one of the single-Cys variants grown under the high-osmolarity (15% sucrose) regime. On the right axis, these CFP/YFP ratios are compared to the Cys-less (C277A) variant. The flipped mutants are highlighted with a red dot in panel A (increased signal output) and a blue dot in panel C (decreased signal output). The shaded areas represent the mean signal output from the Cys-less variant of EnvZ with a range of one standard error of mean. These values are provided to aid in comparison. Error bars represent standard deviation of the mean with a sample size of $n \geq 3$.

Figure 4. Extent of sulfhydryl-reactivity for each single-Cys-containing EnvZ variant. EPB30/pRD400 cells were grown under the low- (empty circles, 0% sucrose) or high-osmolarity (filled circles, 15% sucrose) regimes and subjected to 250 μM molecular iodine for 10 minutes when their OD_{600nm} reached approximately 0.25. As shown in Figure S5, this allowed us to determine the dimer/monomer ratio represented on the Y-axis. Three distinct regions, denoted I, II and III were observed and are described in the text. Error bars represent the standard error of the mean with a sample size of $n \geq 3$.

Figure 5. Aromatic tuning and signal output from EnvZ. (A) When aromatic tuning was performed in EnvZ, a Trp-Leu-Phe triplet (red) was repositioned within the C-terminal region of TM2. (B) Helix displacements, (C) tilt distributions and (D) azimuthal rotational distributions of the aromatically tuned EnvZ TM2 helices. Histograms are shown for all time points of all membranes of each ensemble. Aromatically tuned mutants have been classified based on their signal output as shown in Fig. S6 into

five categories: highly kinase biased (WLF-1; pink), moderately kinase biased (WLF-5, WLF-4, WLF-3; red), balanced (wild-type; black), moderately phosphatase biased (WLF-2, WLF+1, dark blue) and highly phosphatase biased (WLF+2, bright blue).

References

1. Nikaido H. 2003. Molecular basis of bacterial outer membrane permeability revisited. Microbiol Mol Biol Rev 67:593-656.
2. Egger LA, Inouye M. 1997. Purification and characterization of the periplasmic domain of EnvZ osmosensor in Escherichia coli. Biochem Biophys Res Commun 231:68-72.
3. Forst SA, Roberts DL. 1994. Signal transduction by the EnvZ-OmpR phosphotransfer system in bacteria. Res Microbiol 145:363-73.
4. Mizuno T. 1998. His-Asp phosphotransfer signal transduction. J Biochem 123:555-63.
5. Hoch JA, Silhavy TJ (ed). 1995. Two-Component Signal Transduction. American Society of Microbiology Press, Washington, DC, USA.
6. Gerken H, Charlson ES, Cicirelli EM, Kenney LJ, Misra R. 2009. MzrA: a novel modulator of the EnvZ/OmpR two-component regulon. Mol Microbiol 72:1408-22.
7. Gerken H, Misra R. 2010. MzrA-EnvZ interactions in the periplasm influence the EnvZ/OmpR two-component regulon. J Bacteriol 192:6271-8.
8. Forst SA, Delgado J, Inouye M. 1989. DNA-binding properties of the transcription activator (OmpR) for the upstream sequences of ompF in Escherichia coli are altered by envZ mutations and medium osmolarity. J Bacteriol 171:2949-55.
9. Lan CY, Igo MM. 1998. Differential expression of the OmpF and OmpC porin proteins in Escherichia coli K-12 depends upon the level of active OmpR. J Bacteriol 180:171-4.
10. Russo FD, Silhavy TJ. 1991. EnvZ controls the concentration of phosphorylated OmpR to mediate osmoregulation of the porin genes. J Mol Biol 222:567-80.
11. Elliott E, Brink AJ, van Greune J, Els Z, Woodford N, Turton J, Warner M, Livermore DM. 2006. In vivo development of ertapenem resistance in a patient with pneumonia caused by Klebsiella pneumoniae with an extended-spectrum beta-lactamase. Clin Infect Dis 42:e95-8.
12. Hernandez-Alles S, Conejo M, Pascual A, Tomas JM, Benedi VJ, Martinez-Martinez L. 2000. Relationship between outer membrane alterations and susceptibility to antimicrobial agents in isogenic strains of Klebsiella pneumoniae. J Antimicrob Chemother 46:273-7.

13. Jacoby GA, Mills DM, Chow N. 2004. Role of beta-lactamases and porins in resistance to ertapenem and other beta-lactams in Klebsiella pneumoniae. Antimicrob Agents Chemother 48:3203-6.

14. Kaczmarek FM, Dib-Hajj F, Shang W, Gootz TD. 2006. High-level carbapenem resistance in a Klebsiella pneumoniae clinical isolate is due to the combination of bla(ACT-1) beta-lactamase production, porin OmpK35/36 insertional inactivation, and down-regulation of the phosphate transport porin phoe. Antimicrob Agents Chemother 50:3396-406.

15. Loli A, Tzouvelekis LS, Tzelepi E, Carattoli A, Vatopoulos AC, Tassios PT, Miriagou V. 2006. Sources of diversity of carbapenem resistance levels in Klebsiella pneumoniae carrying blaVIM-1. J Antimicrob Chemother 58:669-72.

16. Martinez-Martinez L, Conejo MC, Pascual A, Hernandez-Alles S, Ballesta S, Ramirez De Arellano-Ramos E, Benedi VJ, Perea EJ. 2000. Activities of imipenem and cephalosporins against clonally related strains of Escherichia coli hyperproducing chromosomal beta-lactamase and showing altered porin profiles. Antimicrob Agents Chemother 44:2534-6.

17. Mena A, Plasencia V, Garcia L, Hidalgo O, Ayestaran JI, Alberti S, Borrell N, Perez JL, Oliver A. 2006. Characterization of a large outbreak by CTX-M-1-producing Klebsiella pneumoniae and mechanisms leading to in vivo carbapenem resistance development. J Clin Microbiol 44:2831-7.

18. Adler M, Anjum M, Andersson DI, Sandegren L. 2016. Combinations of mutations in envZ, ftsI, mrdA, acrB and acrR can cause high-level carbapenem resistance in Escherichia coli. J Antimicrob Chemother 71:1188-98.

19. Wang LC, Morgan LK, Godakumbura P, Kenney LJ, Anand GS. 2012. The inner membrane histidine kinase EnvZ senses osmolality via helix-coil transitions in the cytoplasm. EMBO J 31:2648-59.

20. Foo YH, Gao Y, Zhang H, Kenney LJ. 2015. Cytoplasmic sensing by the inner membrane histidine kinase EnvZ. Prog Biophys Mol Biol 118:119-129.

21. Ghosh M, Wang LC, Ramesh R, Morgan LK, Kenney LJ, Anand GS. 2017. Lipid-Mediated Regulation of Embedded Receptor Kinases via Parallel Allosteric Relays. Biophys J 112:643-654.

22. Goulian M. 2010. Two-component signaling circuit structure and properties. Curr Opin Microbiol 13:184-9.

566 23. Jung K, Fried L, Behr S, Heermann R. 2012. Histidine kinases and response regulators in
567 networks. Curr Opin Microbiol 15:118-24.
568 24. Misra R. 2016. Modulators of the bacterial two-component systems involved in evelope stress,
569 transport, and virulence. *In* de Bruijn FJ (ed), Stress and Environmental Regulation of Gene
570 Expression and Adaptation in Bacteria. Wiley-Blackwell, Hoboken, New Jersey, USA.
571 25. Heininger A, Yusuf R, Lawrence R, Draheim RR. 2016. Identification of transmembrane helix
572 1 (TM1) surfaces important for EnvZ dimerisation and signal output. Biochim Biophys Acta\
573 1858:1868-1875.
574 26. Hessa T, Meindl-Beinker NM, Bernsel A, Kim H, Sato Y, Lerch-Bader M, Nilsson I, White
575 SH, von Heijne G. 2007. Molecular code for transmembrane-helix recognition by the Sec61
576 translocon. Nature 450:1026-30.
577 27. Krogh A, Larsson B, von Heijne G, Sonnhammer EL. 2001. Predicting transmembrane protein
578 topology with a hidden Markov model: application to complete genomes. J Mol Biol 305:567-
579 80.
580 28. Zhou Q, Ames P, Parkinson JS. 2009. Mutational analyses of HAMP helices suggest a dynamic
581 bundle model of input-output signalling in chemoreceptors. Mol Microbiol 73:801-14.
582 29. Wright GA, Crowder RL, Draheim RR, Manson MD. 2011. Mutational analysis of the
583 transmembrane helix 2-HAMP domain connection in the Escherichia coli aspartate
584 chemoreceptor tar. J Bacteriol 193:82-90.
585 30. Adase CA, Draheim RR, Manson MD. 2012. The residue composition of the aromatic anchor of
586 the second transmembrane helix determines the signaling properties of the aspartate/maltose
587 chemoreceptor Tar of Escherichia coli. Biochemistry (Mosc)\ 51:1925-32.
588 31. Adase CA, Draheim RR, Rueda G, Desai R, Manson MD. 2013. Residues at the cytoplasmic
589 end of transmembrane helix 2 determine the signal output of the TarEc chemoreceptor.
590 Biochemistry (Mosc)\ 52:2729-38.
591 32. Bass RB, Butler SL, Chervitz SA, Gloor SL, Falke JJ. 2007. Use of site-directed cysteine and
592 disulfide chemistry to probe protein structure and dynamics: applications to soluble and
593 transmembrane receptors of bacterial chemotaxis. Methods Enzymol 423:25-51.
594 33. Draheim RR, Bormans AF, Lai RZ, Manson MD. 2006. Tuning a bacterial chemoreceptor with
595 protein-membrane interactions. Biochemistry (Mosc)\ 45:14655-64.

34. Botelho SC, Enquist K, von Heijne G, Draheim RR. 2015. Differential repositioning of the second transmembrane helices from E. coli Tar and EnvZ upon moving the flanking aromatic residues. Biochim Biophys Acta 1848:615-21.

35. Hall BA, Armitage JP, Sansom MS. 2011. Transmembrane helix dynamics of bacterial chemoreceptors supports a piston model of signalling. PLoS Comput Biol 7:e1002204.

36. Gushchin I, Melnikov I, Polovinkin V, Ishchenko A, Yuzhakova A, Buslaev P, Bourenkov G, Grudinin S, Round E, Balandin T, Borshchevskiy V, Willbold D, Leonard G, Buldt G, Popov A, Gordeliy V. 2017. Mechanism of transmembrane signaling by sensor histidine kinases. Science doi:10.1126/science.aah6345.

37. Hwang E, Cheong HK, Kim SY, Kwon O, Blain KY, Choe S, Yeo KJ, Jung YW, Jeon YH, Cheong C. 2017. Crystal structure of the EnvZ periplasmic domain with CHAPS. FEBS Lett 591:1419-1428.

38. Upadhyay AA, Fleetwood AD, Adebali O, Finn RD, Zhulin IB. 2016. Cache Domains That are Homologous to, but Different from PAS Domains Comprise the Largest Superfamily of Extracellular Sensors in Prokaryotes. PLoS Comput Biol 12:e1004862.

39. Mise T. 2016. Structural Analysis of the Ligand-Binding Domain of the Aspartate Receptor Tar from Escherichia coli. Biochemistry (Mosc)\ 55:3708-13.

40. Norholm MH, von Heijne G, Draheim RR. 2015. Forcing the Issue: Aromatic Tuning Facilitates Stimulus-Independent Modulation of a Two-Component Signaling Circuit. ACS Synth Biol 4:474-81.

41. Batchelor E, Goulian M. 2003. Robustness and the cycle of phosphorylation and dephosphorylation in a two-component regulatory system. Proc Natl Acad Sci U S A 100:691-6.

42. Miyashiro T, Goulian M. 2008. High stimulus unmasks positive feedback in an autoregulated bacterial signaling circuit. Proc Natl Acad Sci U S A 105:17457-62.

43. Siryaporn A, Goulian M. 2008. Cross-talk suppression between the CpxA-CpxR and EnvZ-OmpR two-component systems in E. coli. Mol Microbiol 70:494-506.

44. Chervitz SA, Falke JJ. 1996. Molecular mechanism of transmembrane signaling by the aspartate receptor: a model. Proc Natl Acad Sci U S A 93:2545-50.

45. Falke JJ. 2014. Piston versus Scissors: Chemotaxis Receptors versus Sensor His-Kinase Receptors in Two-Component Signaling Pathways. Structure 22:1219-20.

627 46. Molnar KS, Bonomi M, Pellarin R, Clinthorne GD, Gonzalez G, Goldberg SD, Goulian M, Sali
628 A, DeGrado WF. 2014. Cys-Scanning Disulfide Crosslinking and Bayesian Modeling Probe the
629 Transmembrane Signaling Mechanism of the Histidine Kinase, PhoQ. Structure 22:1239-51.
630 47. Cheung J, Bingman CA, Reyngold M, Hendrickson WA, Waldburger CD. 2008. Crystal
631 structure of a functional dimer of the PhoQ sensor domain. J Biol Chem 283:13762-70.
632 48. Hulko M, Berndt F, Gruber M, Linder JU, Truffault V, Schultz A, Martin J, Schultz JE, Lupas
633 AN, Coles M. 2006. The HAMP domain structure implies helix rotation in transmembrane
634 signaling. Cell\ 126:929-40.
635 49. Inouye M. 2006. Signaling by transmembrane proteins shifts gears. Cell\ 126:829-31.
636 50. Yusuf R, Draheim RR. 2015. Employing aromatic tuning to modulate output from two-
637 component signaling circuits. J Biol Eng 9:7.
638 51. Unnerstale S, Maler L, Draheim RR. 2011. Structural characterization of AS1-membrane
639 interactions from a subset of HAMP domains. Biochim Biophys Acta 1808:2403-12.
640 52. Gushchin I, Gordeliy V. 2018. Transmembrane Signal Transduction in Two-Component
641 Systems: Piston, Scissoring, or Helical Rotation? Bioessays\ 40.
642 53. Falke JJ, Hazelbauer GL. 2001. Transmembrane signaling in bacterial chemoreceptors. Trends
643 Biochem Sci 26:257-65.
644 54. Hazelbauer GL, Falke JJ, Parkinson JS. 2008. Bacterial chemoreceptors: high-performance
645 signaling in networked arrays. Trends Biochem Sci 33:9-19.
646 55. Parkinson JS, Hazelbauer GL, Falke JJ. 2015. Signaling and sensory adaptation in Escherichia
647 coli chemoreceptors: 2015 update. Trends Microbiol 23:257-66.
648 56. Casadaban MJ, Cohen SN. 1980. Analysis of gene control signals by DNA fusion and cloning
649 in Escherichia coli. J Mol Biol 138:179-207.
650 57. Guyer MS, Reed RR, Steitz JA, Low KB. 1981. Identification of a sex-factor-affinity site in E.
651 coli as gamma delta. Cold Spring Harb Symp Quant Biol 45 Pt 1:135-40.
652 58. Batchelor E, Silhavy TJ, Goulian M. 2004. Continuous control in bacterial regulatory circuits. J
653 Bacteriol 186:7618-25.
654 59. Lai RZ, Bormans AF, Draheim RR, Wright GA, Manson MD. 2008. The region preceding the
655 C-terminal NWETF pentapeptide modulates baseline activity and aspartate inhibition of
656 Escherichia coli Tar. Biochemistry (Mosc)\ 47:13287-95.

60. Hsing W, Silhavy TJ. 1997. Function of conserved histidine-243 in phosphatase activity of EnvZ, the sensor for porin osmoregulation in Escherichia coli. J Bacteriol 179:3729-35.

61. Cantwell BJ, Draheim RR, Weart RB, Nguyen C, Stewart RC, Manson MD. 2003. CheZ phosphatase localizes to chemoreceptor patches via CheA-short. J Bacteriol 185:2354-61.

62. Southern JA, Young DF, Heaney F, Baumgartner WK, Randall RE. 1991. Identification of an epitope on the P and V proteins of simian virus 5 that distinguishes between two isolates with different biological characteristics. J Gen Virol 72 (Pt 7):1551-7.

63. Miller JH. 1992. A Short Course in Bacterial Genetics: A Laboratory Manual and Handbook for Escherichia coli and Related Bacteria. Cold Spring Harbor Laboratory Press, Plainview, NY.

64. Ausubel FM, Brent R, Kingston RE, Moore DD, Seidman JG, Smith JA, Struhl K. 1998. Current Protocols in Molecular Biology. Wiley, New York, NY.

65. Schneider CA, Rasband WS, Eliceiri KW. 2012. NIH Image to ImageJ: 25 years of image analysis. Nat Methods 9:671-5.

66. Van Der Spoel D, Lindahl E, Hess B, Groenhof G, Mark AE, Berendsen HJ. 2005. GROMACS: fast, flexible, and free. J Comput Chem 26:1701-18.

674 **Supplemental Information**

675

676 Figure S1. Steady-state expression of EnvZ variants containing a single Cys residue within TM2.
677 EPB30/pRD400 cells expressing one of the single-Cys-containing variants were grown under the low-
678 (0% sucrose) or high-osmolarity (15% sucrose) regimes. Under the low-osmolarity regime, reduced
679 steady-state levels of the D156C variant were observed. In addition, disulfide formation was observed
680 for the F157C and L160C variants in the absence of any additional oxidizing agent. When
681 EPB30/pRD400 cells were grown under the high-osmolarity regime, the F157C, L160C and F161C
682 variants exhibited disulfide formation in the absence of any oxidizing agent.

683

684 Figure S2. Steady-state signal output from the Cys-variant of EnvZ. (A) CFP and YFP fluorescence
685 from MDG147/pEB5 (filled) and EPB30/pRD400 C277A (Cys-less; empty) cells grown under the low-
686 (0% sucrose) and high-osmolarity (15% sucrose) regimes. (B) The CFP/YFP ratio from
687 MDG147/pEB5 (filled) and EPB30/pRD400 C277A (Cys-less; empty) cells grown under the low- and
688 high-osmolarity regimes estimates EmvZ signal output. Error bars represent standard error of the mean
689 with a sample size of $n \geq 3$. Reprinted from BBA Biomembranes, volume 1858, Annika Heininger,
690 Rahmi Yusuf, Robert J. Lawrence and Roger R. Draheim, Identification of transmembrane helix 1
691 (TM1) surfaces important for EnvZ dimerisation and signal output, pages 1868-1875, Copyright 2016,
692 with permission from Elsevier.

693

694 Figure S3. Signal output from the single-Cys-containing EnvZ variants. CFP (A) and YFP (B)
695 fluorescence from EPB30/pRD400 cells expressing one of the receptors from the library grown under
696 the low-osmolarity (0% sucrose) regime. CFP (C) and YFP (D) fluorescence from EPB30/pRD400
697 cells expressing one of the single-Cys-mutants from the library grown under the high-osmolarity (15%
698 sucrose) regime. On the right axes, the ratio of signal output compared to EPB30/pRD400 cells
699 expressing the Cys-less mutant is also presented to aid in comparison. In all panels, the shaded area
700 represents the mean with a range of one standard deviation of the mean from EPB30/pRD400 cells
701 expressing the Cys-less variant of EnvZ (Figure S2). Error bars represent standard error of the mean
702 with an $n \geq 3$.

703

Figure S4. Immunoblotting analysis of the sulfhydryl-reactivity experimentation. EPB30/pRD400 cells expressing one of the single-Cys-containing EnvZ receptors were grown under the low- (0%) or high- (15%) regimes until an OD_{600nm} of approximately 0.25 was reached. Cultures were then subjected to 250 μM molecular iodine. Particular Cys-containing EnvZ receptors resulted in the presence of dimeric EnvZ moieties that migrated at a slower rate than the monomeric species. A minimum of three immunoblots were used for each of the data points present in Figure 3.

Figure S5. Comparison of signal output from osmosensing circuits containing the various aromatically tuned EnvZ receptors. Steady-state signal output from circuits containing the WLF series of aromatically tuned variants expressed in EPB30/pRD400 cells grown under the low (upper panel) or high (lower panel) osmolarity regime is shown. The intracellular levels of phospho-OmpR are estimated through use of the antisymmetrical reporter system presented in Figure S1B. Signal output at low (open circles), medium (gray circles), and high levels (filled circles) of EnvZ-V5 expression (0.2, 0.5, and 0.8, respectively) is presented for comparison. The extent of sensitivity to changes in the amount of EnvZ present is also summarized as robustness. In this column, N/A represents not applicable, as in there is no reasonable amount of signal output, whereas REV indicates reversed, where a decrease in activity is observed as the level of EnvZ-V5 increases. Reprinted from ACS Synthetic Biology, volume 4, Morten Nøholm, Gunnar von Heijne and Roger R. Draheim, Forcing the Issue: Aromatic Tuning Facilitates Stimulus-Independent Modulation of a Two-Component Signaling Circuit, pages 474-481, Copyright 2015, with permission from the American Chemical Society.

Figure S6. A randomly selected (number 63) simulation of the wild-type EnvZ TM2 was selected for demonstration. The blue and cyan dots represent water molecules, while the bronze spheres represent the phosphate in DPPC. The backbone carbon atoms of the peptide are shown pink, while the yellow spheres represent side chains.

Table S1: Mean displacement of the EnvZ TM2 segments in the membrane bilayer.

Table S2: Mean tilt of the EnvZ TM2 segments in the membrane bilayer.

Table S3: Mean azimuthal rotation of the EnvZ TM2 segments in the membrane bilayer.

735

736 Movie S1. A movie composed of frames from the simulation used for Figure S6. To compose the
737 movie, 500 frames spaced 200 ns apart were selected. The blue and cyan dots represent water
738 molecules, while the bronze spheres represent the phosphate in DPPC. The backbone carbon atoms of
739 the peptide are shown pink, while the yellow spheres represent side chains.

740

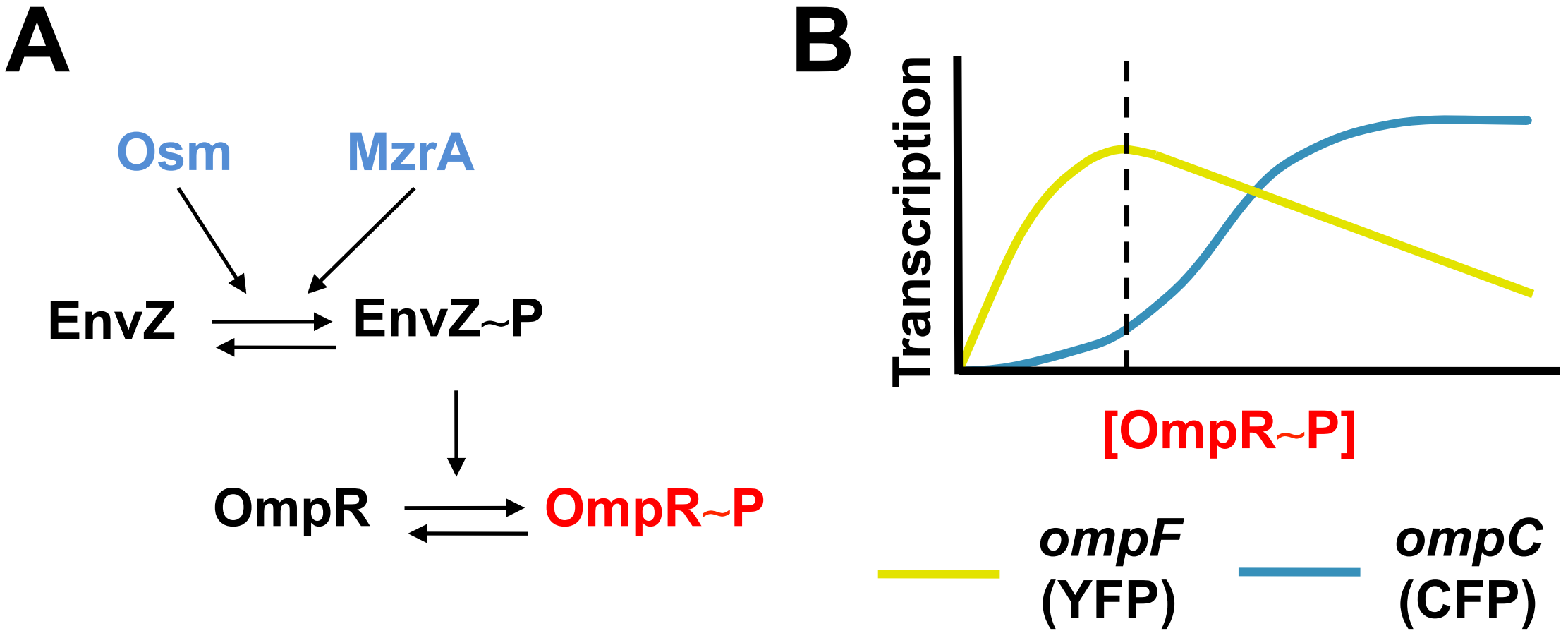
A
Osm
MzrA
EnvZ
EnvZ~P
OmpR
OmpR~P
B
Transcription
[OmpR~P]
ompF
(YFP)
ompC
(CFP)

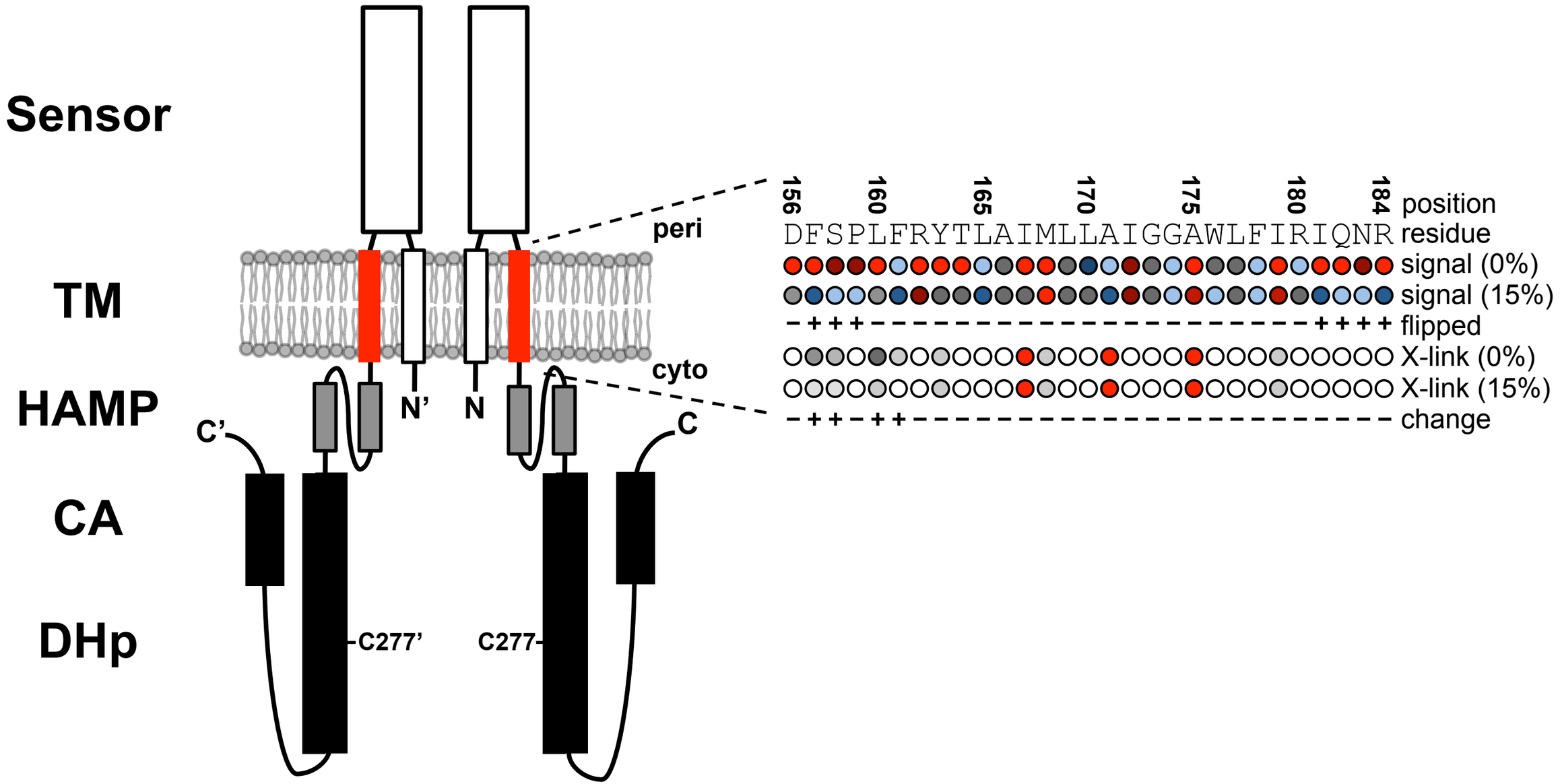
Sensor
TM
HAMP
CA
DHp
peri
cyto
N'
N
C'
C
C277'
C277
156
160
165
170
175
180
184
position
DFSPLFRYTLAIMLLAIGGAWLFIRIQNR
residue
signal (0%)
signal (15%)
flipped
X-link (0%)
X-link (15%)
change

A

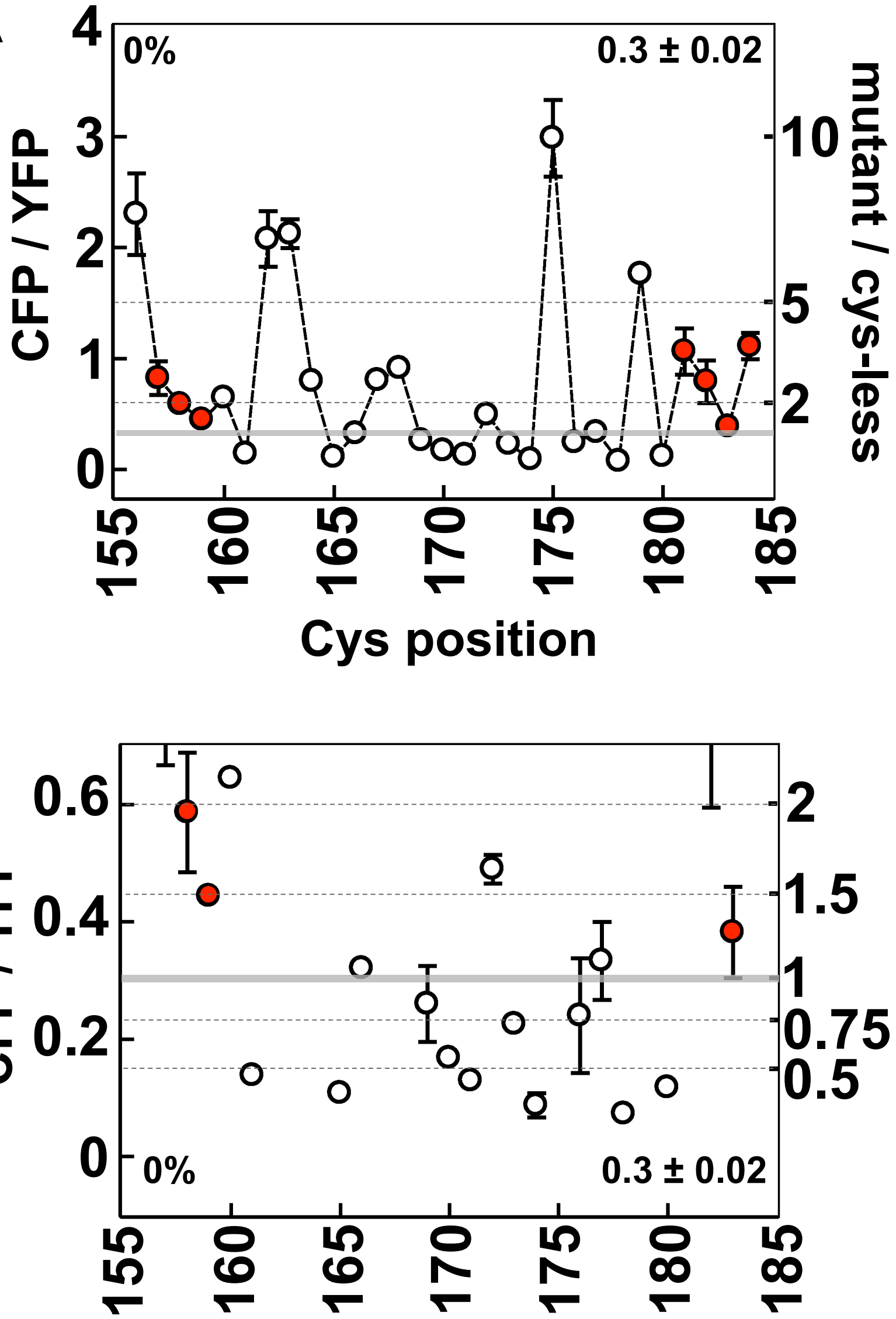
0%
0.3 ± 0.02
CFP / YFP
mutant / cys-less
Cys position
0
1
2
3
4
10
5
2
155
160
165
170
175
180
185

B

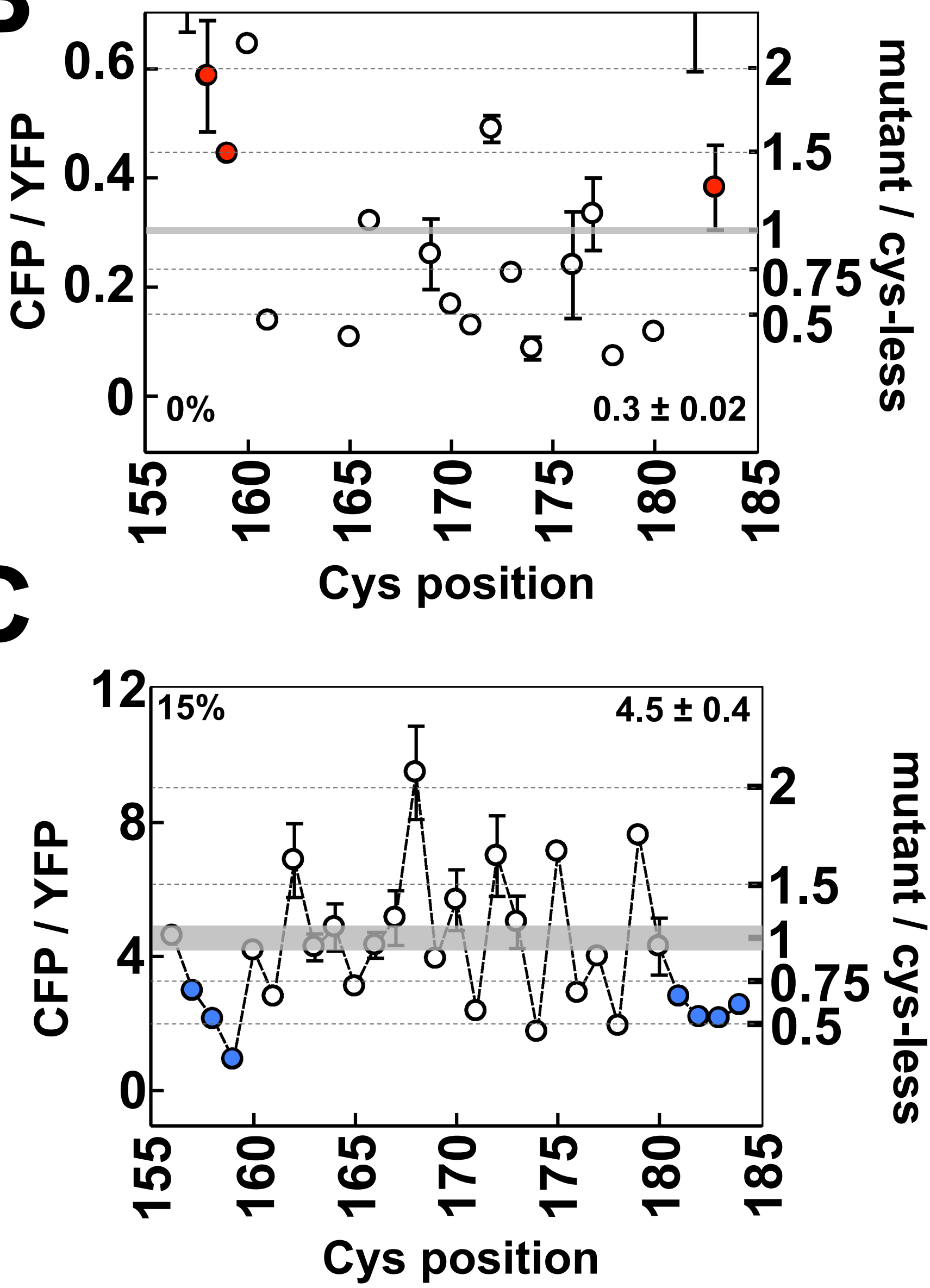
0%
0.3 ± 0.02
CFP / YFP
mutant / cys-less
Cys position
0
0.2
0.4
0.6
2
1.5
1
0.75
0.5
155
160
165
170
175
180
185

C

15%
4.5 ± 0.4
CFP / YFP
mutant / cys-less
Cys position
0
4
8
12
2
1.5
1
0.75
0.5
155
160
165
170
175
180
185

I
II
III
0%
15%
dimer / monomer
3.0
2.5
2.0
1.5
1.0
0.5
0
155
160
165
170
175
180
185
Cys position

A

```
EnvZ WLF-5: IMLLWLFAIGGAIRIQNR
EnvZ WLF-4: IMLLAWLFIGGAIRIQNR
EnvZ WLF-3: IMLLAIWLFGGAIRIQNR
EnvZ WLF-2: IMLLAIGWLFGAIRIQNR
EnvZ WLF-1: IMLLAIGGWLFAIRIQNR
EnvZ WLF 0: IMLLAIGGAWLFIRIQNR
EnvZ WLF+1: IMLLAIGGAGWLFRIQNR
EnvZ WLF+2: IMLLAIGGAGGWLFIQNR
```

B

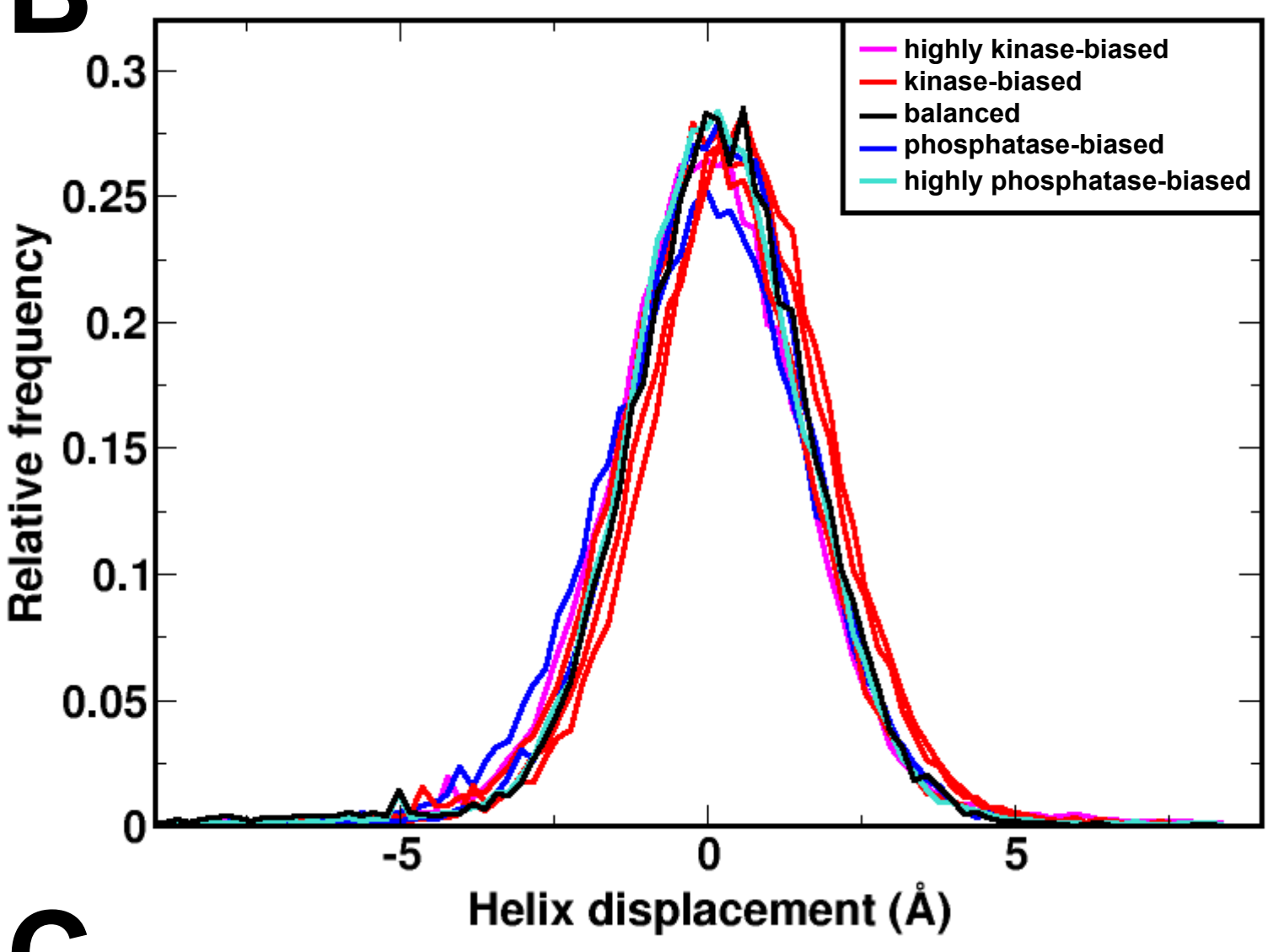

C

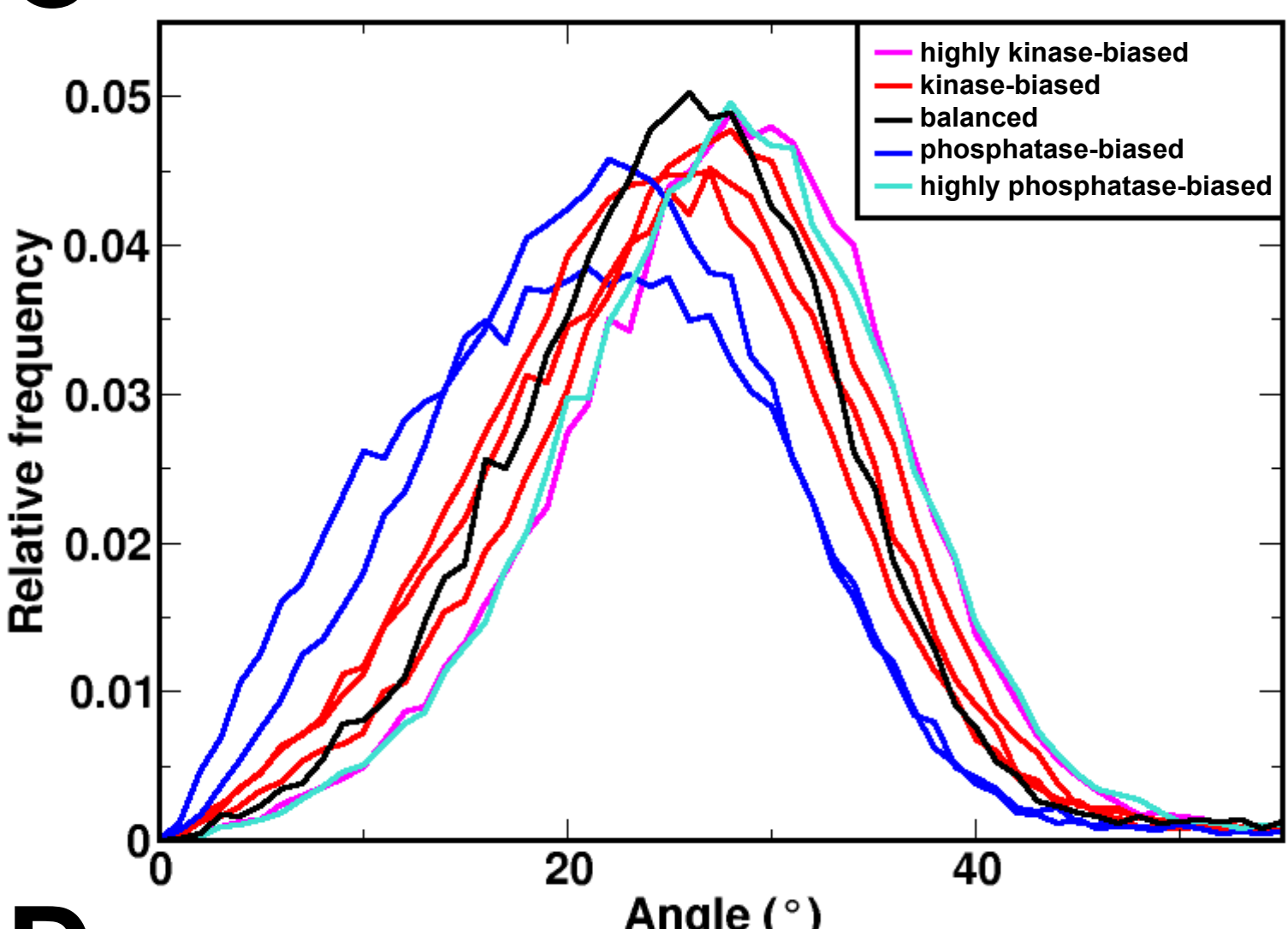

D